Cone-angle Dependence of Ab-initio Structure Solutions Using Precession Electron Diffraction

James Ciston, Christopher S. Own, and Laurence D. Marks

Cone-angle Dependence of *Ab-initio* Structure Solutions Using Precession Electron Diffraction

James Ciston[a], Christopher S. Own[a,b], and Laurence D. Marks[a]

[a]Department of Materials Science and Engineering, Northwestern University
2220 Campus Dr, Evanston, IL 60208, USA
[b]Nion,Co. 1102 8th St., Kirkland, WA 98033, USA

Abstract. Precession electron diffraction (PED) is a technique which is gaining increasing interest due to its ease of use and reduction of the dynamical scattering problem in electron diffraction, leading to more direct structure solutions. We have performed a systematic study of the effect of precession angle for the mineral andalusite on kinematical extinctions and direct methods solutions where the semiangle was varied from 6.5 to 32 mrad in five discrete steps. We show that the intensities of kinematically forbidden reflections decay exponentially as the precession semiangle (φ) is increased and that the amount of information provided by direct methods increases monotonically but non-systematically as φ increases. We have also investigated the zeolite-framework mineral mordenite with PED and have found a direct methods solution where the 12-ring is clearly resolved for the first time.

INTRODUCTION

Precession electron diffraction (PED), originally developed by Vincent and Midgley [1], is a promising technique in electron crystallography that is rapidly becoming mainstream due to the technique's reduction of the dynamical diffraction problem and improvement of transmission electron diffraction measurements. PED datasets have been shown to be "more kinematical" [1-4] due to the avoidance of the strongly excited zone axis condition and the limitation of two-dimensional multiple scattering pathways. One consequence of this is that in many cases kinematically forbidden reflections, which are often very strong in selected-area measurements, exhibit very low intensities in PED experiments, thereby enabling an easier path to symmetry determination and structure solution [5].

Though several studies have theoretically investigated the benefits of using larger cone angles for PED (for example, see [6] and references therein), the majority of experimental studies have utilized a single large cone angle assumed to be sufficient. We have recently published a systematic experimental study exploring the effects of precession cone semiangle (φ) on the intensity of kinematically forbidden reflections, the ease of thickness determination, and the sensitivity of the experimental data to

valence charge density information[7] with the goal of aiding the selection of experimental parameters for future experimental studies. While it is useful to know how forbidden reflections, thickness determination, and sensitivity to charge density behaves as a function of cone angle, the only truly relevant metric for the success of PED is success of solving structures *ab-initio*. Although PED has been shown to yield a more favorable starting guess for structure solution than conventional dynamical diffraction [8, 9] and several new structures have been solved with the use of PED [2, 8, 10-12] (among many other studies), there has yet to be a systematic analysis of how cone angle affects a direct methods phase reconstruction. To this end, we have performed a systematic study of the effect of precession angle for the mineral andalusite on kinematical extinctions and direct methods solutions where the semiangle was varied from 6.5 to 32 mrad in five discrete steps. We show that the amount of information provided by direct methods increases monotonically but non-systematically as φ increases. We have also investigated the zeolite-framework mineral mordenite with PED and have found a direct methods solution where the 12-ring is clearly resolved for the first time.

METHODS AND MATERIALS

Experimental

Andalusite is one of the three polymorphs of Al_2SiO_5 and has an orthorhombic unit cell with a = 7.7980, b = 7.9031, and c = 5.5566 Å and a Pnnm spacegroup (#58) [13]. The sample was prepared of research grade andalusite from a natural mineral source in Santa Theresa, Minas Gerais, Brazil purchased from Ward's Natural Science in the form of ~0.5-5 mm particles. Mordenite is an open framework aluminum silicate zeolite material with a very large unit cell of a = 18.1, b = 20.5, and c = 7.5 Å [14]. Along the [001] direction, mordenite is characterized by 12-rings (a ring of 12 cations and 12 anions alternating) of approximately 45 $Å^2$ projected void space. (Mordenite obtained from Dr. Wharton Sinkler, UOP LLC.) Both samples were crushed and dispersed in ethanol on 300 mesh copper TEM grids coated with lacey carbon.

Experimental PED data was collected using second-generation precession electronics developed at Northwestern University [15]. The precession system was retrofitted to two JEOL microscopes: a 300kv 3000F used for the andalusite experiments, and a 200kv 2000FX microscope used in the mordenite experiments. Both microscopes were equipped with a Gatan US1000 camera which was used with 2x2 binning to produce 1024x1024 pixel images at 16 bits of resolution for data collection.

Numerical

Quantification of diffraction spot intensities was performed using the EDM version 2.0.1 software and InegBZM integration, which is a circular mask linear background algorithm. The andalusite data were quantified using P2mm plane group symmetry (3D space group of Pnnm) to yield 120 symmetry-inequivalent reflections below 1.5

Å^{-1} spatial frequency. The mordenite data were quantified using cmm plane group symmetry (the 3D space group is Cmcm) to yield 182 symmetry-inequivalent reflections below 1 Å^{-1} spatial frequency. Direct methods phase retrieval was also performed using EDM [16, 17].

Precession electron diffraction simulations of the andalusite system were carried out using multislice methods which are described in great detail elsewhere and will not be repeated here [18]. It is important to note that these multislice simulations differ in that they incorporate the full DFT-refined charge density of the unit cell rather than a collection of independent atom scatterers as described in [7].

RESULTS

Results 1: Andalusite

Optimization of Experimental Parameters

The effect of increasing the precession cone angle has been studied theoretically with the general conclusion that a higher angle leads to data which are "better," usually defined as more kinematical, or better-preserving of kinematical intensity ordering [1-4]. It has also been pointed out in several experimental studies that in some cases, the intensities of forbidden reflections are greatly reduced in precession when compared with conventional dynamical intensities and that this effect increases somewhat at larger precession angles[5]. This effect is observed in Andalusite for the (00L), L=2n+1 reflections as shown in Fig. 1 below.

The most notable exception is the case of the (222) reflection of silicon from the original precession paper of Vincent and Midgley [1]. It is useful here to classify the types of reflections which are forbidden and asses what effect (if any) that PED may have on their observability in diffraction patterns.
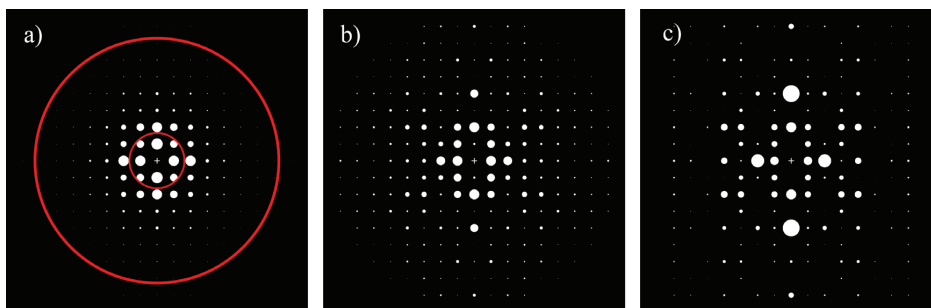
FIGURE 1. a) Experimental zone axis patters and b) experimental 32mrad PED pattern taken along the [110] axis of andalusite. c) Kinematically simulated diffraction pattern. Spot area is proportional to measured intensity. Ring annulus indicates the 0.26-1.26 Å^{-1} range used for direct methods.

a) Extinctions due to glide planes and/or screw axes that do not satisfy the Gjonnes-Moodie orientation conditions [19], and are generally dynamically allowed. These reflections may be excited by a two-dimensional scattering pathway which is less strongly excited in the case of PED.

b) Extinctions due to glide planes and/or screw axes that satisfy the Gjonnes-Moodie orientation conditions [19], and are kinematically and dynamically forbidden on the zone axis and for tilts off the zone which preserve the relevant symmetry operation. Though PED doesn't maintain the relevant symmetry operation along the full circuit of tilts, it is expected that the general reduction of 2-dimensional scattering pathways as in case (a) reduces the observed intensity of these reflections.

c) Accidental forbidden spots such as Si (222) which have a zero structure factor only for spherical atoms, and are not forbidden when bonding effects are included and in general are dynamically allowed. This case exists in the purely kinematical case (i.e. x-ray), but is much more apparent in electron diffraction where bonding effects are more easily observed. This type of extinction is less affected by PED because it does not require a 2-dimensional scattering path as in cases (a) and (b). When a forbidden reflection of this type also lies on a systematic row (as in the specific case of Si(222)), PED may have little effect on the observed intensity.

d) General forbidden reflections due to Wyckoff positions which have a zero structure factor even when bonding effects are included but are dynamically allowed at any orientation. The argument for (a) holds here as well.

e) Unconditional extinctions in which neither dynamical nor kinematical diffraction provide a scattering path, for instance (001) in an fcc material. These extinctions are the result of choosing a non-primitive Bravais lattice and will exhibit zero intensity in both conventional diffraction and PED.

We have recently published a systematic experimental study of the effect of precession cone angle on the intensity of kinematically forbidden reflections in andalusite[7]. Zone axis PED patterns were taken along the [110] direction at cone semiangles of 0, 6.5, 13, 18, 24 and 32 mrad at 300kv. Multislice simulations were also carried out for the same set of cone angles for a range of thicknesses from 2 to 140 nm. The experimental patterns and multislice simulations for a thickness of 102 nm are shown in Fig. 2 below. It is germane to the current discussion to point out the rapid decay of the [001] reflection (and other (00L), L=odd reflections) with increasing cone semiangle. Quantitatively, the decay of the (001) intensity is exponential with a rate constant of -0.109 $1/\varphi$. This rate of decay was calculated from the multislice simulations at 102 nm thickness to be -0.112 $1/\varphi$. Interestingly, the simulated rate of decay appears to be rather invariant of thickness from 28-126 nm at a value of -0.122±0.012 $1/\varphi$.
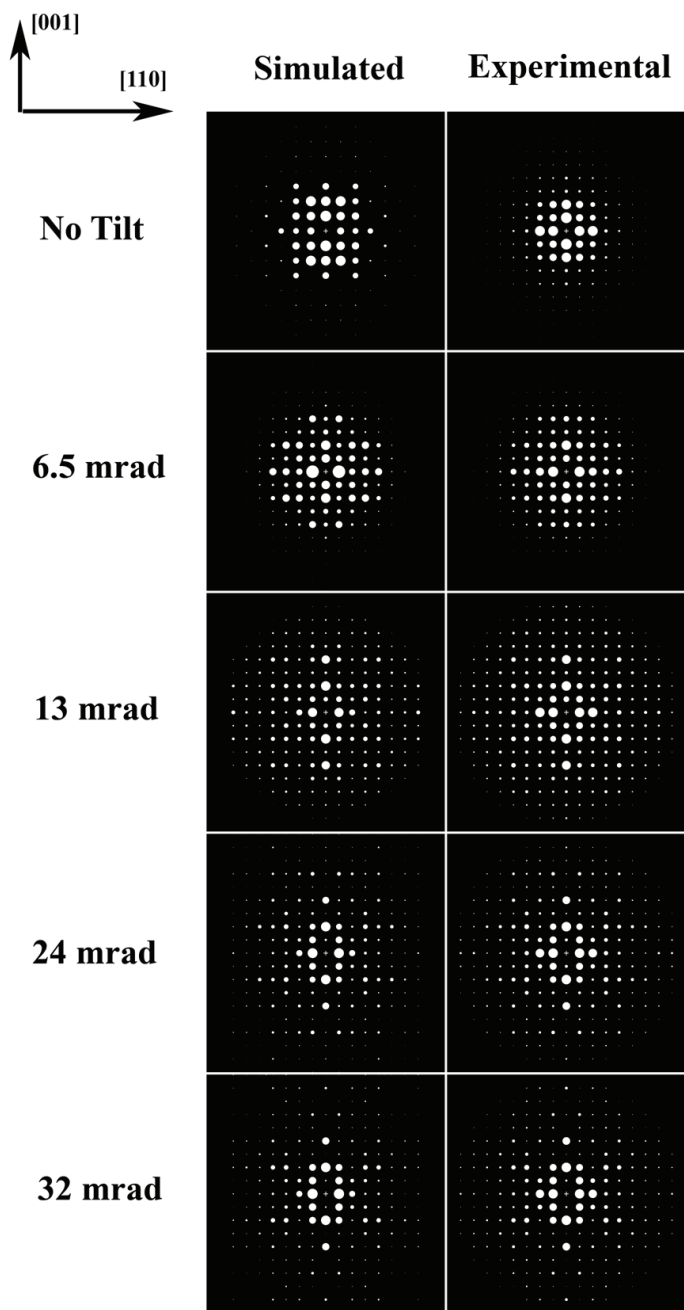
FIGURE 2. Multislice-simulated and experimental diffraction patters for the [110] zone axis of andalusite. Intensity is proportional to circle area. Precession semiangles as indicated. Data reproduced with permission [7].

To determine the true thickness of the sample studied, the experimental intensities were compared to multislice simulations for a range of thickness using the crystallographic R1 figure of merit; these results are shown in Fig. 3. As is well known for dynamical diffraction, the figure of merit as a function of thickness for the unprecessed intensities exhibits numerous non-systematic local minima as a function of thickness making determination of the true sample thickness challenging. As the precession angle increases, the true sample thickness quickly converges to a single minimum indicating 102 nm with a 32 mrad cone angle. This is the thickness used for the multislice simulation shown in the left set of panels in Fig. 2.

Ab-initio Structure Solution

Direct methods are most successful when provided with kinematical structure factors and is taken to be nearly flawless in the case of bulk x-ray diffraction. Although PED leads to experimental data which are often described as "more kinematical," the kinematical approximation has been shown to be insufficient[2]. Repeated analysis using Lorentz-type geometric corrections [1, 20], corrections due to Blackman integration [9, 21, 22], and two-beam approximations [20, 23] indicate that all of these corrections and approximations are inadequate to fully describe the behavior of PED, especially with thick samples.
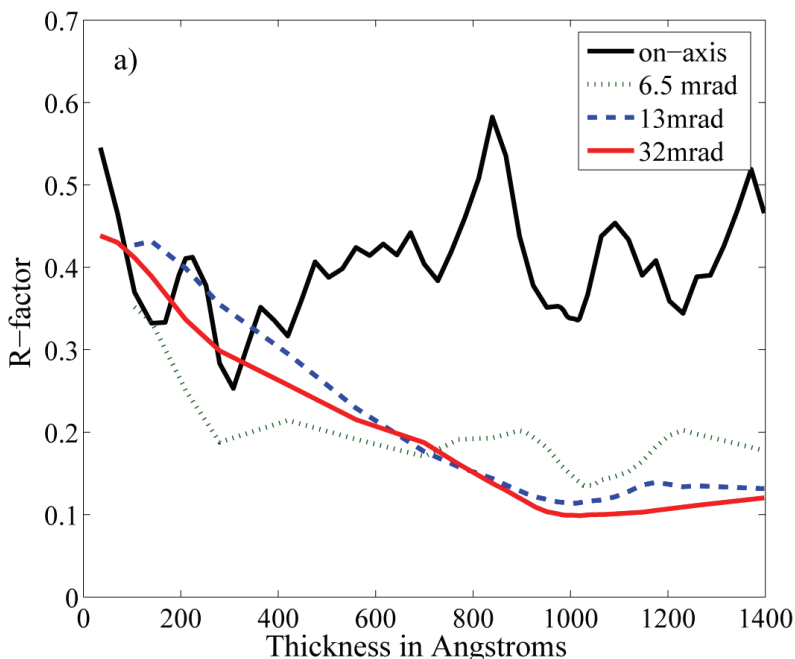
FIGURE 3. R-factor plotted against simulated sample thickness for precession semiangles of 0, 6.5, 13, and 32 mrad. (Semiangles of 18 and 24 mrad omitted for clarity.) Figure reproduced with permission from [7].

Furthermore, the most accurate of these approximations, the 2-beam case, requires some *a-priori* knowledge of the structure in order to perform a forward calculation (though not as much information as a fully dynamical multislice or Bloch wave simulation). We have previously suggested that because geometric effects are most pronounced for low and high scattering vectors, and because large cone angles lead to sufficiently full integration along the excitation error where the Blackman formula takes the limit of $F(g) \sim I(g)$, it is sensible to attempt a structure solution utilizing experimental intensities rather than amplitudes which are bandpass filtered to structurally relevant spatial frequencies of $0.25-1.25 \text{Å}^{-1}$ [8, 24].

EDM direct methods inversion was performed with P2mm symmetry on the datasets shown in Fig 2. Direct methods potential maps of the most probable solution are shown in Fig. 4a for both amplitude and intensity data at all precession semiangles previously described (0, 6.5, 13, 18, 24, and 32 mrad). Note that EDM returns many possible structures (4-18 unique solutions for the 12 runs investigated here), but for unknown structures one must put some faith in the top solutions as being the likeliest candidates for obtaining the correct final refined structure. The total size of each panel is equivalent to 2x2 unit cells with one unit cell centered on each pattern. Figure 4b is a model of the [110] projection of andalusite.

We will begin our analysis by first discussing only the amplitude column of potentials. For low angles of precession, the amplitude generated potential is biased toward what is often referred to as the uranium solution; that is, the resultant potential is dominated by a single strongly scattering feature that does not represent the true structure well. In this case, there is a column of Si atoms at the center of the unit cell, but they are not substantially stronger scatterers than the Al or O atoms elsewhere. As the semiangle increases to 18 mrad, more structure becomes visible in the region surrounding the single bright spot that is evocative of the oxygen atoms around the edge of the unit cell. At 24 mrad, a dramatic change occurs and the potential map strongly exhibits the ring of oxygen atoms around the center and several on the perimeter in addition to the Si column in the center. Only at 32 mrad does one approach the true solution with bright cations populating the perimeter of the unit cell and some bloom from the more weakly scattering oxygen.

Turning to the intensity solutions on the right-hand column of Fig. 4a, the non-precessed (0 mrad) and low angle PED (6.5 mrad) potential maps both have some of the aforementioned character of the uranium solution, but do show potential along the unit cell perimeter. At medium precession semiangles (13 and 18 mrad), the potential does not look much like the projected structure. This is likely due to insufficient sampling along the excitation error for the limit of the Blackman approximation ($F \sim I$) to be valid. At high angles (24 and 32 mrad), the potential map begins to bear striking resemblance to the projected structure. This is especially true of the 32 mrad case where the structure has been overlaid for clarity. While the solutions for amplitude and intensity at 32 mrad are somewhat different from each other, both capture most of the unit cell details. Because the intensity solutions more often seem to produce misleading structures (especially in the middle range of cone angles), it is advisable to use great caution when making this approximation, and reserve its use for large (>30 mrad) semiangles only where integration is more complete.
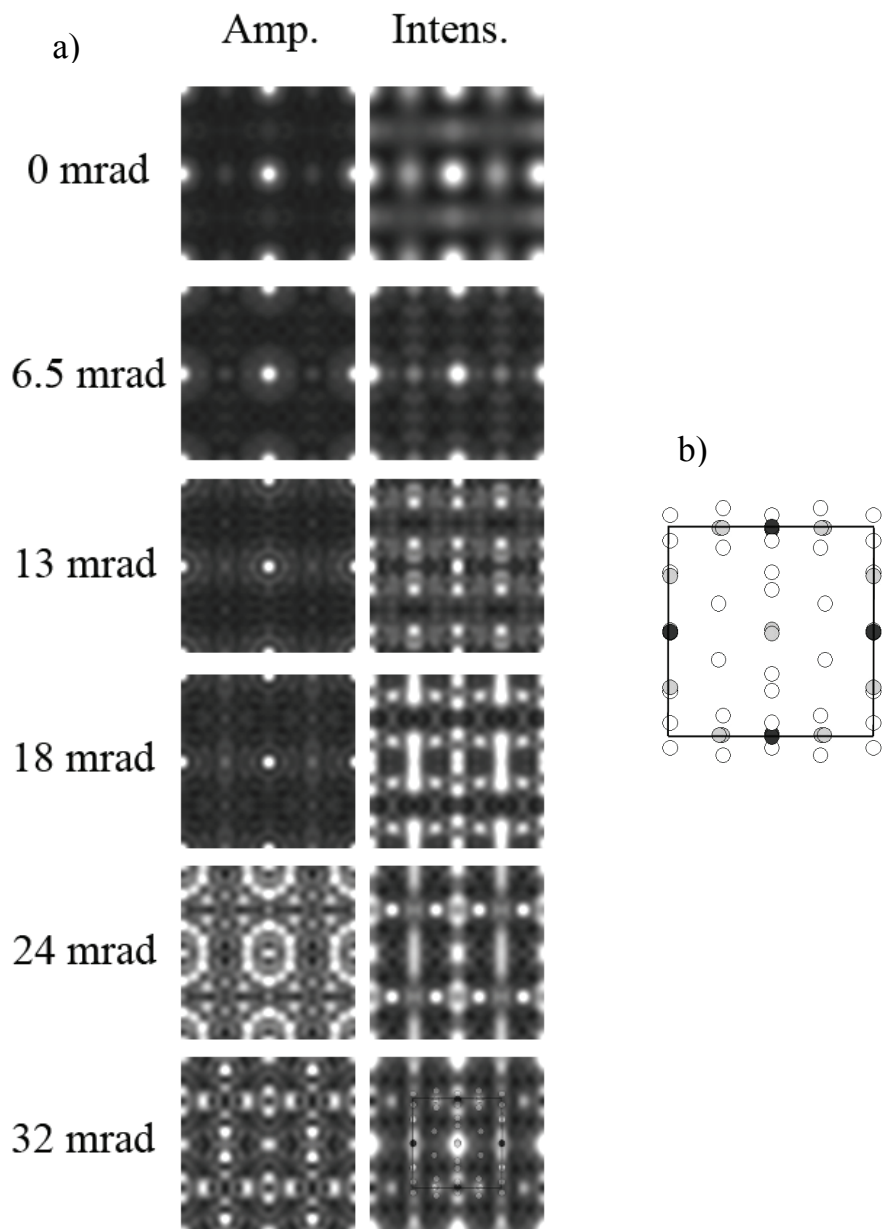
FIGURE 4. a) Potential maps representing the most probable solution from direct methods phase retrieval using the EDM 3.0 software package. The left column was generated using measured structure factor amplitudes (taken to be $\sqrt{I}$) and the right column utilized measured intensities. The lower right panel is overlaid with the projected structure of Andalusite [110] The experimental precession semiangles were as noted. All input data bandpass filtered to 0.26-1.26 Å^{-1} b) projected structure of Andalusite [110], Al=black, Si=grey, O=white. (not to scale)

Results 2: Mordenite

Mordenite is a more challenging material for *ab-initio* solution than andalusite for the following reasons:

1) The structure has a very large unit cell, leading to a large number of structurally-relevant reflections at low scattering angles where effects of the precession geometry are most pronounced.

2) Mordenite is an open-framework zeolite material exhibiting a degree of disorder which leads to very large Debye-Waller temperature factors ($B_{Si} \approx 1.2$ Å and $B_O \approx 3$ Å)

3) Because the structure does not project well, the potential which direct methods must resolve contains more subtle details implying the need for a very accurate experimental dataset.

Precession data was collected for the [001] zone axis of mordenite at 40 mrad semiangle on the 200kv JEOL 2000FX with second-generation precession electronics. The data were quantified using cmm plane group symmetry (the 3D space group is Cmcm) to yield 182 symmetry-inequivalent reflections below 1 Å^{-1} spatial frequency. A conventional diffraction pattern was also collected. Simulated kinematical diffraction data using the aforementioned temperature factors is shown below in Fig. 5 along with the experimental PED data. The agreement between kinematical and experimental data is noticeably worse in this case compared with andalusite from Fig. 1 even though the precession semiangle is larger for mordenite (40 mrad compared with the 32 mrad for andalusite). It is important to point out that the low index experimental reflections are overemphasized due to both geometric and dynamical scattering effects. However, the intensity ordering is relatively preserved.
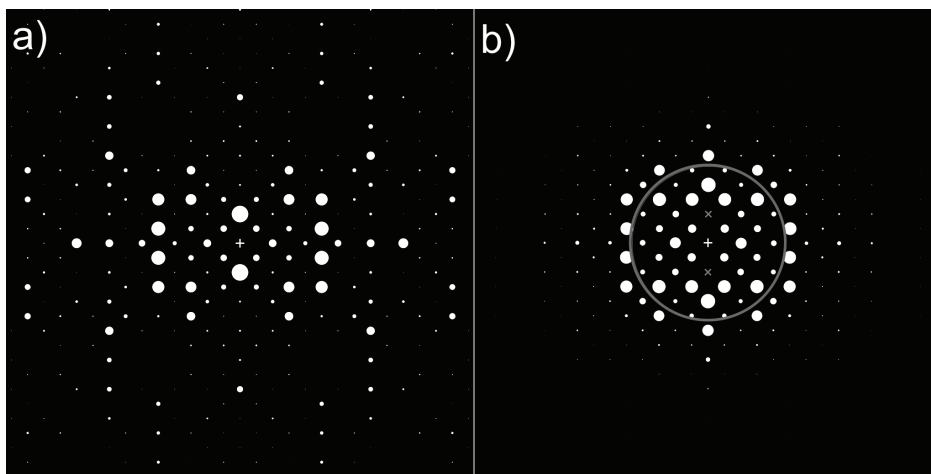

FIGURE 5. a)Simulated kinematical diffraction pattern along the [001] axis of mordenite. b) Experimental precession pattern (200kv, 40 mrad semiangle) of the same zone axis. Ring represents a spatial frequency of 0.25 Å^{-1}. Figure reproduced with permission from [6].

To establish a baseline for the performance of the direct methods algorithm for the mordenite case, a phase retrieval was run with simulated kinematical structure factor amplitudes. The data was truncated to a spatial frequency of 1 Å^{-1} to impose experimental limitations. The resulting potential map is shown in Fig. 6a. Upon careful inspection, it is evident that all cation members and most of the anion members of the 12-ring are clearly resolved as peak-like features in the potential. The potential is overlaid with a structural model of mordenite where the light atoms represent Al/Si and the dark atoms represent oxygen. The vacuum pore space is not completely empty due to truncation of the simulated input data. This simple test case supports the validity of attempting phase retrieval for such a large, poorly projecting structure as mordenite using high quality intensities.

Figure 6b is a direct methods potential map from the experimental PED amplitudes derived from the diffraction intensities shown in Fig. 5b. These amplitudes were not filtered by spatial frequency. The most obvious error in the resulting image is the large potential centered on the pores of the structure, which is unphysical. The general ring structure of this projection is suggested, but there are very few peak-like features to be interpreted as atomic positions around the ring.

A full set of multislice simulations was not performed for the case of mordenite, but the sample exhibited a plate-like morphology with thicknesses of 500-1000 Å. Due to the large sample thickness, we believed that intensities may yield better results from direct methods. In addition, the data was high-pass filtered at 0.25 Å^{-1} which removed a large number of strong reflections which deviate substantially from kinematical behavior. The direct methods analysis produced 4 unique solutions that can be grouped into two distinct families. One family exhibited smeared features in the potential, while the second had a more peak-like character. Figure 7 is the top solution of the second family shown with the contrast reversed. Because there is no absolute reference for the correct phases, it is possible to find a Babinet solution whose phases are the inverse of the true solution resulting in a contrast-reversed image as in this case.
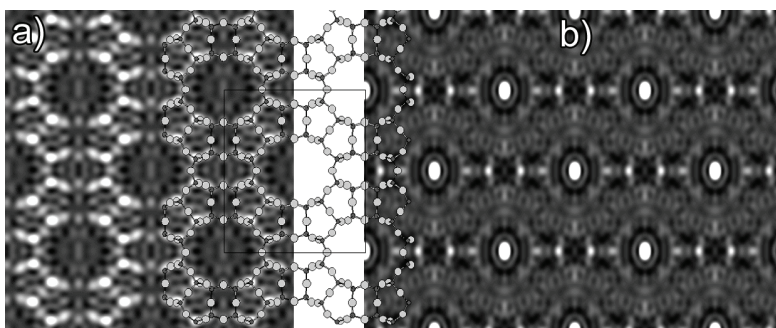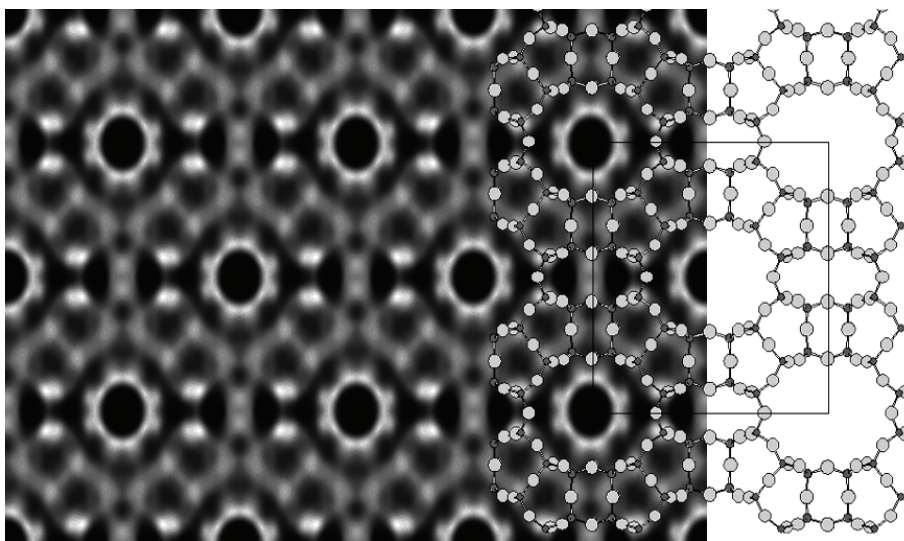

FIGURE 6. a) Potential map from direct methods using kinematical amplitudes low-pass filtered at a spatia1 frequency of 1 Å^{-1} b) Direct methods solution using all measured amplitudes from 40 mrad PED data shown in Figure 5b. Both potential maps overlaid with mordenite structure model (cations light). Figure reproduced with permission from [6].

The potential map in Fig. 7 much more closely matches the true structure of Mordenite. The structure around the pores is more highly resolved than the potential map in Fig. 6b. Of even greater importance, there are 12 distinct features visible around the 12-ring of the pores. This is worth noting because a *ab-initio* solution for mordenite was recently reported from precession electron diffraction data by Dorset *et al* [25] in which only 8 features (all four T-sites) were resolved around the 12-ring. In this solution, there is still a fairly large intensity seen within the pores (though to a much smaller degree than in Fig. 6b). Because this excess potential is concentrated around the perimeter of the ring (rather than in the center) and is periodic, the features may arise from the atoms around the ring having very large anisotropic Debye-Waller factors due to lack of physical constraint. This is similar to the behavior seen at crystal surfaces.

CONCLUSIONS

Precession electron diffraction is a very useful tool for the solution of unknown structures, particularly for crystal phases which are too small to be addressed with conventional x-ray techniques. The semi-empirical assertion that PED is "more kinematical" than conventional electron diffraction has been shown herein to manifest itself in two prominent ways. First, kinematically forbidden reflections of the type exhibited by (00L) of andalusite (those due to n-glide mirror symmetry) decay exponentially with increasing precession cone angle. The rate of decay does not appear to be dependent upon the sample thickness, but this rate (or indeed the exponential behavior) may not transfer to other types of forbidden reflections such as those due to special Wyckoff site occupations or accidental forbidden reflections.

FIGURE 7. Direct methods potential map along mordenite [001] generated from experimental intensities high-pass filtered at 0.25 Å^{-1} spatial frequency. Mordenite structure model overlays image. Figure reproduced with permission from [6].

Also for the case of andalusite, increasing the precession angle also increases the amount of information conveyed from direct methods phasing, though this occurs in a non-systematic fashion. Larger precession angles may lead to more information in a recovered potential map, but not always the same kind of information, as exhibited by the appearance of oxygen atoms for the very specific semiangle of 24 mrad in Fig. 4a. One should also be careful using intensities rather than amplitudes for direct methods when the precession angle is not sufficiently large for full integration of the excitation error.

In the case of mordenite, the cone angle was sufficiently large (40 mrad semiangle) that the direct methods potential map from high-pass filtered intensities clearly resolved the 12-ring along the [001] axis of mordenite. Conversely, the potential derived from unfiltered amplitudes was grossly insufficient to convey peaks indicating projected atomic positions.

In general, we recommend utilizing the largest feasible cone angle if *ab-inito* structure solution is to be attempted from PED data. However, care must be taken that microscope aberrations at high angle do not distort the diffraction spots to such a degree that quantification becomes impossible.

ACKNOWLEDGMENTS

REFERENCES

1. R. Vincent and P. A. Midgley, Ultramicroscopy **53**, p. 271-82 (1994).
2. J. Gjonnes, V. Hansen, B. S. Berg, et al., Acta Crystallogr. Sect. A **54**, p. 306-19 (1998).
3. C. S. Own, L. D. Marks, and W. Sinkler, Acta Crystallogr. Sect. A **62**, p. 434-43 (2006).
4. A. Avilov, K. Kuligin, S. Nicolopoulos, et al., Ultramicroscopy **107**, p. 431-44 (2007).
5. J. P. Morniroli, A. Redjaimia, and S. Nicolopoulos, Ultramicroscopy **107**, p. 514-22 (2007).
6. C. S. Own, "System Design and Verification of the Precession Electron Diffraction Technique", Ph.D. Thesis, Northwestern University, 2005
7. J. Ciston, B. Deng, L. D. Marks, et al., Ultramicroscopy, In Press, Corrected Proof, doi:10.1016/j.ultramic.2007.08.004, p. 1-9 (2007).
8. C. S. Own, W. Sinkler, and L. D. Marks, Ultramicroscopy **106**, p. 114-22 (2006).
9. C. S. Own, A. K. Subramanian, and L. D. Marks, Microscopy and Microanalysis **10**, p. 96-104 (2004).
10. M. Gemmi, X. D. Zou, S. Hovmoller, et al., Acta Crystallogr. Sect. A **59**, p. 117-26 (2003).
11. T. E. Weirich, J. Portillo, G. Cox, et al., Ultramicroscopy **106**, p. 164-75 (2006).
12. K. Boulahya, L. Ruiz-Gonzalez, M. Parras, et al., Ultramicroscopy **107**, p. 445-52 (2007).
13. J. K. Winter and S. Ghose, American Mineralogist **64**, p. 573-86 (1979).
14. C. Baerlocher, W. M. Meier, and D. H. Olson, in *Atlas of Zeolite Framework Types* (Elsevier, 2001), 190-91.
15. C. S. Own, L. D. Marks, and W. Sinkler, Rev. Sci. Instrum. **76**, p. 033703:1-13 (2005).
16. R. Kilaas, L. D. Marks, and C. S. Own, Ultramicroscopy **102**, p. 233-37 (2005).
17. R. Kilaas, C. S. Own, B. Deng, et al., EDM: Electron Direct Methods: Documentation-2.0.1, <http://www.numis.northwestern.edu/edm/documentation/edm.htm>, (2006)
18. C. S. Own, L. D. Marks, and W. Sinkler, Acta Crystallographica Section A **62**, p. 434-43 (2006).
19. J. Gjonnes and A. F. Moodie, Acta Crystallogr. **19**, p. 65-67 (1965).
20. K. Gjonnes, Ultramicroscopy **69**, p. 1-11 (1997).
21. M. Blackman, Proc. Roy. Soc. **173**, p. 68-82 (1939).
22. D. L. Dorset, in *Structural Electron Crystallography* (Plenum Publishing, New York, 1995), p. 179.
23. W. Sinkler, C. S. Own, and L. D. Marks, Ultramicroscopy **107**, p. 543-50 (2007).
24. W. Sinkler, L. D. Marks, D. D. Edwards, et al., Journal of Solid State Chemistry **136**, p. 145-49 (1998).
25. D. L. Dorset, C. J. Gilmore, J. L. Jorda, et al., Ultramicroscopy **107**, p. 462-73 (2007).